

1 **Aerosol pH and its driving factors in Beijing**

2 **Jing Ding², Pusheng Zhao^{1*}, Jie Su¹, Qun Dong¹, Xiang Du^{2, 1}, and Yufen Zhang²**

3 ¹ Institute of Urban Meteorology, China Meteorological Administration, Beijing 100089, China

4 ² State Environmental Protection Key Laboratory of Urban Ambient Air Particulate Matter Pollution
5 Prevention and Control, College of Environmental Science and Engineering, Nankai University,
6 Tianjin 300071, China

7 * *Correspondence to:* P. S. Zhao (pszhao@ium.cn)

8 **Abstract**

9 Aerosol acidity plays a key role in secondary aerosol formation. The long-term high-temporal
10 resolution PM_{2.5} pH and size-resolved aerosol pH in Beijing were calculated with ISORROPIA-II.
11 In 2016-2017, the mean PM_{2.5} pH (at relative humidity (RH) > 30%) over four seasons was 4.5±0.7
12 (winter) > 4.4±1.2 (spring) > 4.3±0.8 (autumn) > 3.8±1.2 (summer), showing moderate acidity. In
13 coarse-mode aerosols, Ca²⁺ and Mg²⁺ played an important role in aerosol pH. Under heavily polluted
14 conditions, more secondary ions accumulated on the coarse particles, leading to a change in the
15 acidity of the coarse particles from neutral to weakly acidic. Sensitivity tests also demonstrated the
16 significant contribution of crustal ions to PM_{2.5} pH. In the North China Plain (NCP), the common
17 driving factors affecting PM_{2.5} pH variation in all four seasons were SO₄²⁻, TNH₃ (total ammonium
18 (gas+aerosol)), and temperature, while the unique factors were Ca²⁺ in spring and RH in summer.
19 Elevated SO₄²⁻ levels can enhance aerosol acidity due to the stronger ability of SO₄²⁻ to provide
20 hydrogen ions. The decreasing SO₄²⁻ and increasing NO₃⁻ mass fractions in PM_{2.5} as well as
21 excessive NH₃ in the atmosphere in the NCP in recent years are the reasons why aerosol acidity in
22 China is lower than that in Europe and the United States. The nonlinear relationship between PM_{2.5}
23 pH and TNH₃ indicated that although NH₃ in the NCP was abundant, the PM_{2.5} pH was still acidic,
24 which might be attributed to the limited aerosol liquid water content (ALWC) and hydrolysis of
25 ammonium salts. Elevated RH values can enhance water uptake and promote gas-to-particle
26 conversion. Therefore, the specific impact of RH on PM_{2.5} pH needs to be determined by the degrees
27 of change in H_{air}⁺ and ALWC. Gas-particle partitioning sensitivity tests revealed that the typical
28 high RH values and low temperatures during haze events in the NCP are conducive to the formation
29 of secondary particles. To reduce nitrate by controlling ammonia, the amount of ammonia must be
30 greatly reduced below excessive quantities.

31 **Key words:** Aerosol pH, ISORROPIA-II, Influencing factors, Beijing

32

33 **1. Introduction**

34 Aerosol acidity has a significant effect on secondary aerosol formation through the gas-aerosol
35 partitioning of semi-volatile and volatile species (Eddingsaas et al., 2010; Surratt et al., 2010; Pathak
36 et al., 2011a; Guo et al., 2016). Studies have shown that aerosol acidity can promote the generation
37 of secondary organic aerosols by affecting aerosol acid-catalysed reactions (Rengarajan et al., 2011).
38 Moreover, metals can become soluble by acid dissociation under low aerosol pH (Shi et al., 2011;
39 Meskhidze et al., 2003) or by forming ligands with organic species, such as oxalate, at higher pH
40 (Schwertmann et al., 1991). In addition, high aerosol acidity can lower the buffer capacity and affect
41 the formation of acid rain. The investigation of aerosol acidity is conducive to better understanding
42 the important role of aerosols in acid deposition and atmospheric chemical reactions.

43 Aerosol acidity is frequently estimated by the charge balance of measurable cations and anions
44 in the aerosol liquid phase. A net negative balance is correlated with acidic aerosols and vice versa
45 (Zhang et al., 2007; Pathak et al., 2011b; Zhao et al., 2017). Generally, a larger ion balance value
46 implies stronger acidity or stronger alkalinity. Nevertheless, ion balance and other similar proxies
47 fail to represent the in situ aerosol pH because such metrics cannot accurately predict the H^+
48 concentration in the aerosol liquid phase (Guo et al., 2015; Hennigan et al., 2015). To better
49 understand the in situ aerosol pH, the aerosol liquid water content (ALWC) and hydrogen ion
50 concentration per volume air (H_{air}^+) should be determined (Guo et al., 2015).

51 Most inorganic ions and some organic acids in aerosols are water soluble (Peng, 2001; Wang et
52 al., 2017). Since the deliquescence relative humidity (DRH) of mixed salts is lower than that of any
53 single component, ambient aerosols are generally in the form of droplets containing liquid water
54 (Seinfeld and Pandis, 2016). ALWC can be derived from hygroscopic growth factors or calculated
55 by thermodynamic models, and good consistencies in ALWC have been found among these methods
56 (Engelhart et al., 2011; Bian et al., 2014; Guo et al., 2015). However, H_{air}^+ can only be obtained by
57 thermodynamic models, which offer a more precise approach to determine aerosol pH (Nowak et
58 al., 2006; Fountoukis et al., 2009; Weber et al., 2016; Fang et al., 2017). Among these
59 thermodynamic models, ISORROPIA-II is widely used owing to its rigorous calculation,
60 performance, and computational speed (Guo et al., 2015; Fang et al., 2017; Liu et al., 2017; Galon-
61 Negru et al., 2018).

62 The North China Plain (NCP) is the region with the most severe aerosol pollution in China.
63 Nitrate and sulfate are the major contributors to haze, and their secondary formation processes are
64 determined in large part by aerosol pH (Zou et al., 2018; Huang et al., 2017; Gao et al., 2018).
65 Therefore, understanding the aerosol pH level in this region is extremely important and has recently
66 become a trending topic. Some studies conducted in the NCP showed that the aerosol acidity was
67 close to neutral (Cheng et al., 2016; Wang et al., 2016; Chi et al., 2017), while in some other studies,
68 fine particles showed moderate acidity (Liu et al., 2017; Shi et al., 2017). These results all indicated
69 significantly higher pH values than those found in the United States or Europe, where aerosols are
70 often highly acidic with a pH lower than 3.0 (Guo et al., 2015, 2016; Bougiatioti et al., 2016; Weber

71 et al., 2016; Young et al., 2013). The differences in aerosol pH in the NCP arise from 1) different
72 methods or different model settings, 2) variations in PM_{2.5} chemical composition in the NCP in
73 recent years, 3) the levels of gas precursors of the main water-soluble ions (NH₃, HNO₃, and HCl),
74 and 4) differences in ambient temperature and relative humidity (RH). In some countries where the
75 particulate matter concentration is very low, pH diurnal variations are mainly driven by
76 meteorological conditions (Guo et al., 2015, 2016; Bougiatioti et al., 2016). In the NCP, a
77 comprehensive understanding of the impacts of these factors on aerosol pH is still poor.

78 Additionally, most studies on aerosol pH focus on PM₁ or PM_{2.5}. Knowledge regarding size-
79 resolved aerosol pH is still rare. Aerosol chemical compositions are different among multiple size
80 ranges. Among inorganic ions, SO₄²⁻, NO₃⁻, Cl⁻, K⁺, and NH₄⁺ are mainly concentrated in the fine
81 mode except on dusty days (Meier et al., 2009; Pan et al., 2009; Tian et al., 2014), whereas Mg²⁺
82 and Ca²⁺ are abundant in the coarse mode (Zhao et al., 2017). Aerosol pH can be expected to be
83 diverse among different particle sizes; pH levels at different sizes may be associated with different
84 formation pathways of secondary aerosols.

85 To better understand the driving factors of aerosol acidity, in this work, the thermodynamic model
86 ISORROPIA-II was utilized to predict aerosol pH in Beijing based on a long-term online high-
87 temporal resolution dataset and a size-resolved offline dataset. The hourly measured PM_{2.5} inorganic
88 ions and precursor gases in four seasons from 2016 to 2017 were used to analyse the seasonal and
89 diurnal variations in aerosol acidity; samples collected by multi-stage cascade impactors (MOUDI-
90 120) were used to estimate the pH variations among 10 different size ranges. Additionally, a
91 sensitivity analysis was conducted to identify the key factors affecting aerosol pH and gas-particle
92 partitioning. The main purposes of this work are to 1) obtain the PM_{2.5} pH level based on long-term
93 online aerosol samples, contributing towards a global pH dataset; 2) investigate the size-resolved
94 aerosol pH, providing useful information for understanding the formation processes of secondary
95 aerosols; and 3) explore the main factors affecting aerosol pH and gas-particle partitioning, which
96 can help explain the possible reasons for pH divergence in different works and provide a basis for
97 controlling secondary aerosol generation.

98 **2. Data Collection and Methods**

99 **2.1 Site**

100 The measurements were performed at the Institute of Urban Meteorology in the Haidian district
101 of Beijing (39°56'N, 116°17'E). The site is located next to a high-density residential area, without
102 significant nearby air pollution emissions. Therefore, the observation data represent the air quality
103 levels of the urban area of Beijing.

104 **2.2 Online data collection**

105 Water-soluble ions (SO₄²⁻, NO₃⁻, Cl⁻, NH₄⁺, Na⁺, K⁺, Mg²⁺, and Ca²⁺) in PM_{2.5} and gaseous
106 precursors (HCl, HNO₃, HNO₂, SO₂, and NH₃) in ambient air were measured by an online analyser
107 (MARGA) with hourly temporal resolution during spring (April and May 2016), winter (February
108 2017), summer (July and August 2017), and autumn (September and October 2017). More details

109 about MARGA can be found in Rumsey et al. (2014) and Chen et al. (2017). The PM_{2.5} and PM₁₀
110 mass concentrations (TEOM 1405DF), hourly ambient temperature and RH were also
111 synchronously obtained. The hourly concentrations of PM_{2.5}, PM₁₀, and major secondary ions (SO₄²⁻,
112 NO₃⁻, and NH₄⁺) in PM_{2.5}, as well as meteorological parameters during the observations, are shown
113 in Figure 1. In the spring, two dust events occurred (April 21 and May 6). In the following pH
114 analysis based on MARGA data, it was assumed that the particles were internally mixed; hence,
115 these two dust events were excluded from this analysis.

116 **Figure 1**

117 **2.3 Size-resolved chemical composition**

118 A micro-orifice uniform deposit impactor (MOUDI-120) was used to collect size-resolved aerosol
119 samples with calibrated 50% cut sizes of 0.056, 0.10, 0.18, 0.32, 0.56, 1.0, 1.8, 3.1, 6.2, 9.9 and 18
120 μm. Size-resolved sampling was conducted July 12-18, 2013; January 13-19, 2014; July 3-5, 2014;
121 October 9-20, 2014; and January 26-28, 2015. Fifteen, fourteen, and eighteen sets of samples were
122 obtained in summer, autumn, and winter, respectively. Except for two sets of samples, all the
123 samples were collected in daytime (from 08:00 to 19:00) and nighttime (from 20:00 to 7:00 the next
124 day). One hour of preparation time was allowed for filter changing and washing the nozzle plate
125 with ethanol. The water-soluble ions in the samples were analysed by using ion chromatography
126 (DIONEX ICS-1000). Detailed information about the features of MOUDI-120 and the procedures
127 of sampling, pre-treatment, and laboratory chemical analysis (including quality assurance & quality
128 control) were described in our previous papers (Zhao et al., 2017; Su et al., 2018). Gas precursors
129 were not observed during the periods of MOUDI sampling.

130 **2.4 Aerosol pH prediction**

131 Aerosol pH can be predicted by thermodynamic models such as AIM and ISORROPIA (Clegg et al.
132 et al., 1998; Nenes et al., 1998). AIM is considered an accurate benchmark model, while ISORROPIA
133 has been optimized for use in chemical transport models. Currently, ISORROPIA-II, with the
134 addition of K⁺, Mg²⁺, and Ca²⁺ (Fountoukis and Nenes, 2007), can calculate the equilibrium H_{air}⁺
135 and ALWC with reasonable accuracy by using the water-soluble ion mass concentration,
136 temperature (T), and RH as input. H_{air}⁺ and ALWC were then used to predict aerosol pH by Eq. (1).

$$137 \quad \text{pH} = -\log_{10} H_{\text{aq}}^+ \cong -\log_{10} \frac{1000 H_{\text{air}}^+}{ALWC_i} \quad (1)$$

138 where H_{aq}⁺ (mole L⁻¹) is the hydronium ion concentration in the ambient particle liquid water. H_{aq}⁺
139 can also be calculated as H_{air}⁺ (μg m⁻³) divided by the concentration of ALWC associated with
140 inorganic species, ALWC_i (μg m⁻³). Both the inorganic species and part of the organic species in
141 particles are hygroscopic. However, pH prediction is not highly sensitive to water uptake by organic
142 species (ALWC_o) (Guo et al., 2015, 2016). In recent years, the fraction of organic matter in PM_{2.5} in
143 the NCP was 20%~25%, which is much lower than that in the United States (Guo et al., 2015). In
144 contrast, approximately 50% of PM_{2.5} in the NCP is inorganic ions (Huang et al., 2017; Zhang et al.,
145 2018; Zhang et al., 2019). The results obtained by Liu et al. (2017) in Beijing showed that the mass

146 fraction of organic matter-induced particle water accounted for only 5% of total ALWC, indicating
147 a negligible contribution to aerosol pH. Hence, aerosol pH can be fairly well predicted by
148 ISORROPIA-II with only measurements of inorganic species in most cases. However, potential
149 errors can be incurred by ignoring $ALWC_0$ in regions where hygroscopic organic species have a
150 relatively high contribution to fine particles.

151 In ISORROPIA-II, forward and reverse modes are provided to predict ALWC and H_{air}^+ . In
152 forward mode, T, RH, and the total (*i.e.*, gas+aerosol) concentrations of NH_3 , H_2SO_4 , HCl, and
153 HNO_3 need to be input. In reverse mode, equilibrium partitioning is calculated given only the
154 concentrations of aerosol components, RH, and T as input. In this work, the online ion
155 chromatography system MARGA was used to measure both inorganic ions in $PM_{2.5}$ and gaseous
156 precursors. Moreover, the forward mode has been reported to be less sensitive to measurement error
157 than the reverse mode (Hennigan et al., 2015; Song et al., 2018). Hence, ISORROPIA-II was run in
158 forward mode for aerosols in the metastable conditions in this study.

159 When using ISORROPIA-II to calculate the $PM_{2.5}$ acidity, all particles were assumed to be
160 internally mixed, and the bulk properties were used without considering the variability in chemical
161 composition with particle size. In the ambient atmosphere, the aerosol chemical composition is
162 complicated; hence, the deliquescence relative humidity (DRH) of aerosols is generally low
163 (Seinfeld and Pandis, 2016), and particles usually exist in the form of droplets, which makes the
164 assumption that the particles are in a liquid state (metastable condition) reasonable. However, when
165 particles are exposed to a substantially low RH, the state of the particles may change. Figure 2 and
166 Figure S1-S4 show comparisons between the predicted and measured NH_3 , HNO_3 , HCl, NH_4^+ , NO_3^- ,
167 Cl^- , $\epsilon(NH_4^+)$ ($NH_4^+/(NH_3+NH_4^+)$, mol/mol), $\epsilon(NO_3^-)$ ($NO_3^-/(HNO_3+NO_3^-)$, mol/mol), and $\epsilon(Cl^-)$
168 ($Cl^-/(HCl+Cl^-)$, mol/mol) based on real-time ion chromatography data; all results are coloured with
169 the corresponding RH. The predicted and measured NH_3 , NH_4^+ , NO_3^- , and Cl^- values are in good
170 agreement: the R^2 values of linear regressions are all higher than 0.94, and the slopes are
171 approximately 1. Moreover, the agreement between the predicted and measured $\epsilon(NH_4^+)$ is better
172 than those of $\epsilon(NO_3^-)$ and $\epsilon(Cl^-)$. The slope of the linear regression between the predicted and
173 measured $\epsilon(NH_4^+)$ was 0.93, 0.91, 0.95, and 0.96 and R^2 was 0.87, 0.93, 0.89, and 0.97 in spring,
174 winter, summer, and autumn, respectively. However, the measured and predicted partitioning of
175 HNO_3 and HCl show significant discrepancies (R^2 values of 0.28 and 0.18, respectively), which
176 may be attributed to the much lower gas concentrations than particle concentrations, as well as the
177 HNO_3 and HCl measurement uncertainties from MARGA (Rumsey et al., 2014). Clearly, more
178 scatter points deviate from the 1:1 line when ISORROPIA-II is operated at $RH \leq 30\%$, which is
179 highly evident in winter and spring. For data with $RH \leq 30\%$, the predictions are significantly
180 improved when assuming the aerosols are in stable mode (solid + liquid) (Figure S5-S6) and the
181 aerosol liquid water is almost zero and cannot be used to predict aerosol pH. This behaviour reveals
182 that it is not reasonable to predict aerosol pH using the thermodynamic model when the RH is
183 relatively low. Consequently, we only determined the $PM_{2.5}$ pH for data with RH values higher than

184 30% in this work.

185

Figure 2

186 Running ISORROPIA-II in the forward mode with only aerosol component concentrations as
187 input may result in a bias in predicted pH due to repartitioning of ammonia in the model, leading to
188 a lower predicted pH when gas-phase data are not available (Hennigan et al., 2015). In this work,
189 no gas phase was available for size-resolved pH prediction. We determined aerosol pH through an
190 iteration procedure that used the measured particulate species and ISORROPIA-II to predict gas
191 species. Detailed information can be found in Fang et al. (2017) and Guo et al. (2016). In summary,
192 the predicted NH_3 , HNO_3 , and HCl concentrations from the $i-1$ th run were applied to the i th iteration
193 until the gas concentrations converged. Based on these iterative gas-phase concentrations, the ion
194 concentrations of samples collected by MOUDI as well as the average RH and T during each
195 sampling period were used to determine the aerosol pH for different size ranges. Similar to
196 calculating the $\text{PM}_{2.5}$ pH, it was assumed that all the particles in each size bin were internally mixed
197 and had the same pH.

198 Comparisons of the iterative and predicted NH_3 , HNO_3 , and HCl as well as the measured and
199 predicted NO_3^- , NH_4^+ , Cl^- , $\epsilon(\text{NH}_4^+)$, $\epsilon(\text{NO}_3^-)$, and $\epsilon(\text{Cl}^-)$ for MOUDI samples are shown in Figure
200 3. A previous study showed that coarse-mode particles could not easily reach equilibrium with
201 gaseous precursors due to kinetic limitations (Dassios et al., 1999; Cruz et al., 2000). Assuming that
202 coarse-mode particles are in equilibrium with the gas phase could result in a large bias between the
203 measured and predicted NO_3^- and NH_4^+ in coarse-mode particles (Fang et al., 2017). Additionally,
204 in this work, assuming that coarse-mode particles are in equilibrium with the gas phase could over-
205 predict NO_3^- and Cl^- and underestimate NH_4^+ in the coarse mode (blue scatters), which could
206 subsequently underestimate the coarse-mode aerosol pH. In contrast to the coarse-mode particles,
207 the measured and predicted NO_3^- , NH_4^+ , and Cl^- agreed very well in fine-mode particles.
208 Considering the kinetic limitations and nonideal gas-particle partitioning in coarse-mode particles,
209 the aerosol pH in the coarse mode was determined by ignoring the gas phase.

210

Figure 3

211 2.5 Sensitivity of $\text{PM}_{2.5}$ pH to SO_4^{2-} , TNO_3 , TNH_3 , Ca^{2+} , RH, and T

212 To explore the major influencing factors on aerosol pH, sensitivity tests were performed. In the
213 sensitivity analysis, SO_4^{2-} , TNO_3 (total nitrate (gas+aerosol) expressed as equivalent HNO_3), TNH_3
214 (total ammonium (gas+aerosol) expressed as equivalent NH_3), Ca^{2+} , RH, and T were selected as the
215 variables since SO_4^{2-} and NO_3^- are major anions in aerosols, NH_4^+ and Ca^{2+} are major cations in
216 aerosols, and Ca^{2+} is generally considered representative of crustal ions. To assess how a variable
217 affects $\text{PM}_{2.5}$ pH, the real-time measured values of this variable and the average values of other
218 variables in each season were input into ISORROPIA-II. The magnitude of the relative standard
219 deviation (RSD) of the calculated aerosol pH can reflect the impact of variable variations on aerosol
220 acidity. The higher the RSD is, the greater the impact, and vice versa. The average value and
221 variation range for each variable in the four seasons are listed in Table S1.

222 The sensitivity analysis in this work was only aimed at PM_{2.5} (*i.e.*, fine particles) since the
223 MARGA system equipped with a PM_{2.5} inlet had a high temporal resolution (1 h). In addition, the
224 data set had a wide range, covering different levels of haze events. The sensitivity analysis in this
225 work only reflected the characteristics during the observation periods, and further work is needed
226 to determine whether the sensitivity analysis is valid in other environments.

227 **3. Results and Discussion**

228 **3.1 Overall summary of PM_{2.5} pH over four seasons**

229 The average mass concentrations of PM_{2.5} and major inorganic ions in the four seasons are shown
230 in Table 1. Among all the ions measured, NO₃⁻, SO₄²⁻, and NH₄⁺ were the three most dominant
231 species, accounting for 83% ~ 87% of the total ion content. The average concentrations of primary
232 inorganic ions (Cl⁻, Na⁺, K⁺, Mg²⁺, and Ca²⁺) were higher in spring than in other seasons. PM_{2.5} in
233 Beijing showed moderate acidity, with PM_{2.5} pH values of 4.4±1.2, 4.5±0.7, 3.8±1.2, and 4.3±0.8
234 for spring, winter, summer, and autumn observations, respectively (data at RH ≤30% were excluded).
235 The overall winter PM_{2.5} pH was comparable to the result (4.2) found in Beijing by Liu et al. (2017)
236 and that (4.5) found by Guo et al. (2017), but lower than that (4.9, winter and spring) in Tianjin (Shi
237 et al., 2017), another mega city approximately 120 km away from Beijing. The PM_{2.5} pH in summer
238 was lowest among all four seasons. The seasonal variation in PM_{2.5} pH in this work was similar to
239 the results in Tan et al. (2018), except for spring, and followed the trend winter (4.11 ± 1.37) >
240 autumn (3.13 ± 1.20) > spring (2.12 ± 0.72) > summer (1.82 ± 0.53).

241 **Table 1**

242 To further investigate the PM_{2.5} pH level under different pollution conditions over four seasons,
243 the PM_{2.5} concentrations were classified into three groups: 0~75 μg m⁻³, 75~150 μg m⁻³, and >150
244 μg m⁻³, representing clean, polluted, and heavily polluted conditions, respectively. The relationship
245 between PM_{2.5} concentration and pH is shown in Figure S7. The PM_{2.5} pH under clean conditions
246 spanned 2~7, while those under polluted and heavily polluted conditions was mostly concentrated
247 from 3~5. Table 1 shows that as the air quality deteriorated, the aerosol component concentration,
248 as well as ALWC and H_{air}⁺, all increased in each season. The average PM_{2.5} pH under clean
249 conditions was the highest (Table 1), followed by polluted and heavily polluted conditions in spring,
250 summer, and autumn. In winter, however, the average pH under polluted conditions (4.8±1.0) was
251 the highest.

252 On clean days, a higher PM_{2.5} pH (>6) was generally accompanied by a higher mass fraction of
253 crustal ions (Mg²⁺ and Ca²⁺), while a lower PM_{2.5} pH (<3) was accompanied by a higher mass
254 fraction of SO₄²⁻ and lower mass fraction of crustal ions; such conditions were most obvious in
255 summer (Figure 4). Under polluted and heavily polluted conditions, the mass fractions of major
256 chemical components were similar, and the difference in PM_{2.5} pH between these two conditions
257 was also small. All of these results indicated that the aerosol chemical composition might be the
258 essential factor that drives aerosol acidity. The impact of aerosol composition on PM_{2.5} pH is
259 discussed in Section 3.4.

Figure 4

In spring, summer, and autumn, the pH of PM_{2.5} from the northern direction was generally higher than that from the southwest direction, but the higher pH in summer also occurred with strong southwest winds (wind speed >3 m s⁻¹) (Figure 5). Generally, northern winds occur with cold-front systems, which can sweep away air pollutants but raise dust in which the crustal ion species (Ca²⁺, Mg²⁺) are higher. In winter, the PM_{2.5} pH was distributed relatively evenly in all wind directions, but we surprisingly found that the pH in northerly winds could be as low as 3~4, which was consistent with the high mass fraction of SO₄²⁻ on clean days caused by the northern winds.

Figure 5

3.2 Diurnal variation in ALWC, H_{air}⁺, and PM_{2.5} pH

Obvious diurnal variation was observed based on the long-term online dataset, as shown in Figure 6. To understand the factors that can drive changes in PM_{2.5} pH, the diurnal variations of NO₃⁻, SO₄²⁻, ALWC, and H_{air}⁺ were investigated and are exhibited in Figure 6. Generally, ALWC was higher during nighttime than daytime and reached a peak near 04:00 ~ 06:00 (local time). After sunrise, the increasing temperature resulted in a rapid drop in RH, leading to a clear loss of particle water, and ALWC reached the lowest level in the afternoon. H_{air}⁺ was highest in the afternoon, followed by nighttime, and H_{air}⁺ was relatively low in the morning. The low ALWC and high H_{air}⁺ values in the afternoon resulted in the minimum pH at this time. The average nighttime pH was 0.3~0.4 units higher than that during daytime. The diurnal variations in PM_{2.5} pH described here were determined for the cases with an RH higher than 30%.

The correlation between NO₃⁻ concentration and PM_{2.5} pH was weakly positive at low ALWC, and PM_{2.5} pH was almost independent of the NO₃⁻ mass concentration at higher ALWC values (Figure S8). In contrast, at a low ALWC level, increasing SO₄²⁻ decreased the pH; at a high ALWC level, a negative correlation still existed between SO₄²⁻ mass concentration and PM_{2.5} pH. SO₄²⁻ had a greater effect than NO₃⁻ on PM_{2.5} pH.

Figure 6

From the above discussion, we found that both H_{air}⁺ and ALWC had significant diurnal variations, indicating that aerosol acidity in the NCP was driven by both aerosol composition and particle water. This trend is slightly different from the situation from the US: Guo et al. (2015) found that the ALWC diurnal variation was significant and the diurnal pattern in pH was mainly driven by the dilution of aerosol water. Specifically, in winter, the PM_{2.5} mass concentration in Beijing was several times or even dozens of times higher than that in the US, and the RH was generally low, which means there were more seeds in the limited particle water. Hence, the dilution of H_{air}⁺ by aerosol liquid water was quite limited in winter.

3.3 Factors affecting PM_{2.5} pH

In this work, the effects of SO₄²⁻, TNO₃, TNH₃, Ca²⁺, RH, and T on PM_{2.5} pH were determined through a four-season sensitivity analysis. The common important driving factors affecting PM_{2.5} pH variations in all four seasons were SO₄²⁻, TNH₃, and T (Table 2), while the unique influencing

298 factors were Ca^{2+} in spring and RH in summer. For ALWC, the most important factor was RH,
299 followed by SO_4^{2-} or NO_3^- . Figure 7 and Figure S9-S16 show how these factors affect the $\text{PM}_{2.5}$ pH,
300 ALWC, and H_{air}^+ over all four seasons.

301

Table 2

302 Theoretically, elevated TNO_3 can reduce $\text{PM}_{2.5}$ pH since the $\text{HNO}_3 \rightarrow \text{NO}_3^-$ conversion process
303 can release H^+ . However, in the sensitivity tests, we found that only the $\text{PM}_{2.5}$ pH in winter and
304 autumn decreased significantly with elevated TNO_3 (Figure 7, S16). In spring and summer, $\text{PM}_{2.5}$
305 pH changed little with elevated TNO_3 . Moreover, when the TNO_3 concentration was low, $\text{PM}_{2.5}$ pH
306 even increased with elevated TNO_3 (Figure 7, S13). The phenomenon was mainly due to the rich-
307 ammonia condition in the NCP (Figure S18). The sensitivity tests showed that elevated TNH_3 could
308 consume H_{air}^+ swiftly and increase the $\text{PM}_{2.5}$ pH. In this work, the lower TNH_3 mass concentration
309 in winter and higher TNO_3 mass concentration in autumn (Table S1) resulted in decreased $\text{PM}_{2.5}$ pH
310 with elevated TNO_3 . In spring and summer, excessive NH_3 could continuously buffer the increasing
311 TNO_3 , leading to the minimal changes in $\text{PM}_{2.5}$ pH. Changes in TNH_3 in the lower concentration
312 range had a significant impact on $\text{PM}_{2.5}$ pH, and changes in TNH_3 at higher concentrations could
313 only generate limited pH changes (Figure 7, S13, S16). The nonlinear relationship between $\text{PM}_{2.5}$
314 pH and TNH_3 indicates that although NH_3 in the NCP was abundant, the $\text{PM}_{2.5}$ pH was far from
315 neutral, which might be attributed to the limited ALWC. Compared to the liquid water content in
316 clouds and precipitation, the ALWC was much lower; hence, the dilution of H_{air}^+ by aerosol liquid
317 water was limited. Moreover, the hydrolysis of ammonium salts contributes to the release of
318 hydrogen ions.

319

Figure 7

320 Compared with NO_3^- , SO_4^{2-} has a key role in aerosol acidity due to its stronger ability to provide
321 H^+ during the $\text{H}_2\text{SO}_4 \rightarrow \text{SO}_4^{2-}$ conversion process (Figure S9, S11, S14). Hence, elevated SO_4^{2-} is
322 crucial in the increase of H_{air}^+ . In this work, $\text{PM}_{2.5}$ pH was lowest in summer but highest in winter,
323 which was consistent with the SO_4^{2-} mass fraction with respect to the total ion content. The SO_4^{2-}
324 mass fraction was highest in summer among the four seasons, with a value of $32.4\% \pm 11.1\%$, but
325 lowest in winter, with a value of $20.9\% \pm 4.4\%$. In recent years, the SO_4^{2-} mass fraction in $\text{PM}_{2.5}$ in
326 Beijing has decreased significantly due to the strict emission control measures for SO_2 ; in most
327 cases, NO_3^- dominates the inorganic ions (Zhao et al., 2013, 2017; Huang et al., 2017; Ma et al.,
328 2017), which could reduce aerosol acidity. A study in the Pearl River Delta of China showed that
329 the in situ acidity of $\text{PM}_{2.5}$ significantly decreased from 2007-2012; the variation in acidity was
330 mainly caused by the decrease in sulfate (Fu et al., 2015). The excessive NH_3 in the atmosphere and
331 the high NO_3^- mass fraction in $\text{PM}_{2.5}$ may be the reason why the aerosol acidity in China is lower
332 than that in Europe and the United States. In addition, the DRH of NH_4NO_3 is lower than that of
333 $(\text{NH}_4)_2\text{SO}_4$ (Seinfeld and Pandis, 2016); hence, the particles dominated by NH_4NO_3 can deliquesce
334 at lower RH, which may result in the increase in ALWC.

335 Ca^{2+} is an important crustal ion; in the output of ISORROPIA-II, Ca exists mainly as CaSO_4

336 (slightly soluble). Elevated Ca^{2+} concentrations can increase $\text{PM}_{2.5}$ pH by decreasing H_{air}^+ and
337 ALWC (Figure 7 and Figure S9-S16). As discussed in Section 3.1, on clean days, $\text{PM}_{2.5}$ pH reached
338 6~7 when the mass fraction of Ca^{2+} was high; hence, the role of crustal ions on $\text{PM}_{2.5}$ pH cannot be
339 ignored in areas or seasons (such as spring) in which mineral dust is an important particle source.
340 Due to the strict control measures for road dust, construction sites, and other bare ground, the crustal
341 ions in $\text{PM}_{2.5}$ decreased significantly in the NCP, especially on polluted days.

342 In addition to the particle chemical composition, meteorological conditions also have important
343 impacts on aerosol acidity. RH had a different impact on $\text{PM}_{2.5}$ pH in different seasons. Elevated
344 RH can enhance water uptake and promote gas-to-particle conversion. In winter, the H_{air}^+ increase
345 caused by elevated RH was much larger than the increase in ALWC; hence, elevated RH could
346 reduce $\text{PM}_{2.5}$ pH. However, an opposite tendency was observed in summer due to the lower mass
347 concentration of chemical components, and the dilution effect of ALWC on H_{air}^+ was obvious only
348 in summer (Figure 7). In spring and autumn, RH had little impact on $\text{PM}_{2.5}$ pH due to the
349 synchronous variation in H_{air}^+ and ALWC (Figure S13, S16). The different impacts of RH on $\text{PM}_{2.5}$
350 pH indicated that the higher RH during severe haze may increase aerosol acidity. Temperature can
351 alter the $\text{PM}_{2.5}$ pH by affecting gas-particle partitioning. At higher ambient temperatures, $\epsilon(\text{NH}_4^+)$,
352 $\epsilon(\text{NO}_3^-)$, and $\epsilon(\text{Cl}^-)$ all showed a decreased tendency (Figure 8). The volatilization of ammonium
353 nitrate and ammonium chloride can result in a net increase in particle H^+ and lower pH (Guo et al.,
354 2018). Moreover, a higher ambient temperature tends to lower ALWC, which can further decrease
355 $\text{PM}_{2.5}$ pH.

356 **Figure 8**

357 **3.4 Size distribution of aerosol pH values**

358 Inorganic ions in particles present clear size distributions, and the size-resolved chemical
359 composition can change at different pollution levels (Zhao et al., 2017; Ding et al., 2017; Ding et
360 al., 2018), which may result in variations in aerosol pH. Thus, we further investigated the size-
361 resolved aerosol pH at different pollution levels. According to the average $\text{PM}_{2.5}$ concentration
362 during each sampling period, all the samples were also classified into three groups (clean, polluted,
363 and heavily polluted) according to the rules described in Section 3.1. A severe haze episode occurred
364 during the autumn sampling period; hence, there were more heavily polluted samples in autumn
365 than in other seasons. Figure 9 shows the average size distributions of PM components and pH under
366 clean, polluted, and heavily polluted conditions in summer, autumn, and winter. NO_3^- , SO_4^{2-} , NH_4^+ ,
367 Cl^- , K^+ , OC, and EC were mainly concentrated in the size range of 0.32~3.1 μm , while Mg^{2+} and
368 Ca^{2+} were predominantly distributed in the coarse mode (>3.1 μm). During haze episodes, the
369 sulfate and nitrate in the fine mode increased significantly. However, the increases in Mg^{2+} and Ca^{2+}
370 in the coarse mode were not as substantial as the increases in NO_3^- , SO_4^{2-} , and NH_4^+ , and the low
371 wind speed made it difficult to raise dust during heavily polluted periods. More detailed information
372 about the size distributions for all analysed species during the three seasons is given in Zhao et al.
373 (2017) and Su et al. (2018).

Figure 9

The aerosol pH in both the fine mode and coarse mode was lowest in summer among the three seasons, followed by autumn and winter. The seasonal variation in aerosol pH derived from MOUDI data was consistent with that derived from the real-time PM_{2.5} dataset. In summer, the predominance of sulfate in the fine mode and high ambient temperature resulted in a low pH, ranging from 1.8 to 3.9. The fine-mode aerosol pH in autumn and winter was in the range of 2.4 ~ 6.3 and 3.5 ~ 6.5, respectively. In the fine mode, the difference in aerosol pH among size bins was not significant, probably owing to the excessive NH₃ (Guo et al., 2017). Additionally, the size distributions of aerosol pH in the daytime and nighttime were explored and are illustrated in Figure S19. In summer and autumn, the pH in the daytime was lower than that in the nighttime, while in winter, the pH was higher in the daytime. During the winter sampling periods, SO₄²⁻ and NO₃⁻ were obviously higher and led to abundant H_{air}⁺ in the nighttime.

The abundance of Ca²⁺ and Mg²⁺ in the coarse mode led to a predicted coarse particle pH approximately at or higher than 7 for all three seasons. The difference in aerosol pH (with and without Ca²⁺ and Mg²⁺) increased with increasing particle size above 1 μm (Figure S20). Moreover, the coarse-mode aerosols during severely hazy days shifted from neutral to weakly acidic, especially in autumn and winter. As shown in Figure 9, the pH in stage 3 (3.1-6.2 μm) declined from 7.8 (clean) to 4.5 (heavily polluted) in winter. The significant decrease in the mass ratios of Ca²⁺ and Mg²⁺ in the coarse mode on heavily polluted days resulted in the loss of acid-buffering capacity. Furthermore, the different size-resolved aerosol acidity levels may be associated with different generation pathways of secondary aerosols. According to Cheng et al. (2017) and Wang et al. (2017), the aqueous oxidation of SO₂ by NO₂ is key in sulfate formation under a high RH and neutral conditions. However, it is speculated that dissolved metals or HONO may be more important for secondary aerosol formation under acidic conditions.

3.5 Factors affecting gas-particle partitioning

Gas-particle partitioning can be directly affected by the concentration levels of gaseous precursors and meteorological conditions. In this work, sensitivity tests showed that decreasing TNO₃ lowered ε(NH₄⁺) effectively, which helped maintain NH₃ in the gas phase. Elevated TNH₃ can increase ε(NO₃⁻) when TNO₃ is fixed, which means that the elevated TNH₃ altered the gas-particle partitioning and shifted more TNO₃ into the particle phase, leading to an increase in nitrate (Figure 8 and S17). Controlling the emissions of both NO_x (gaseous precursor of NO₃⁻) and NH₃ are efficient ways to reduce NO₃⁻. However, the relationship between TNH₃ and ε(NO₃⁻) in the sensitivity tests (Figure 8 and S17) showed that the ε(NO₃⁻) response to TNH₃ control was highly nonlinear, which means that a decrease in nitrate would happen only when TNH₃ is greatly reduced. The same result was also obtained from a study by Guo et al. (2018). The main sources of NH₃ emission are agricultural fertilization, livestock, and other agricultural activities, which are all associated with people's livelihoods. Therefore, in terms of controlling the generation of nitrate, a reduction in NO_x emissions is more feasible than a reduction in NH₃ emissions.

412 RH and temperature can also alter gas-particle partitioning. The equilibrium constants for
413 solutions of ammonium nitrate or ammonium chloride are functions of T and RH. The measurement
414 data also showed that lower T and higher RH contribute to the conversion of more TNH_3 , TNO_3 ,
415 and TCl into the particle phase (Table 3). When the RH exceeded 60%, more than 90% of TNO_3
416 was in the particle phase for all four seasons. In summer and autumn, lower RH was generally
417 accompanied by higher ambient temperature, and more than half of the TNO_3 and TCl were
418 partitioned into the gaseous phase. In contrast, in winter and spring, low temperatures favoured the
419 reduction of NO_3^- and volatilization of Cl^- , and $\varepsilon(\text{NO}_3^-)$ and $\varepsilon(\text{Cl}^-)$ were higher than 65%, even at
420 low RH; $\varepsilon(\text{NH}_4^+)$ was lower than $\varepsilon(\text{NO}_3^-)$ and $\varepsilon(\text{Cl}^-)$. In spring, summer, and autumn, the average
421 $\varepsilon(\text{NH}_4^+)$ was still lower than 0.3 even when the RH was >60%; this trend was associated with excess
422 NH_3 in the NCP. In summary, higher RH and lower temperature are favourable conditions for the
423 formation of secondary particles, which are typical meteorological characteristics of haze events in
424 the NCP (Figure 1); hence, gaseous precursor emission control is crucially important.

425 **Table 3.**

426 **5. Summary and Conclusions**

427 Long-term high-temporal resolution $\text{PM}_{2.5}$ pH and size-resolved aerosol pH in Beijing were
428 calculated with ISORROPIA-II. The model validation results indicated that it is not reasonable to
429 assume aerosols are in a liquid state (metastable) when the RH is lower than 30%. In 2016-2017 in
430 Beijing, the mean $\text{PM}_{2.5}$ pH (RH>30%) over four seasons was 4.5 ± 0.7 (winter) > 4.4 ± 1.2 (spring) >
431 4.3 ± 0.8 (autumn) > 3.8 ± 1.2 (summer), showing moderate acidity. In this work, both H_{air}^+ and ALWC
432 had significant diurnal variations, indicating that aerosol acidity in the NCP was driven by both
433 aerosol composition and meteorological conditions. The average $\text{PM}_{2.5}$ nighttime pH was 0.3~0.4
434 units higher than that in the daytime. The $\text{PM}_{2.5}$ pH in northerly wind was generally higher than that
435 in wind from the southwest. Size-resolved aerosol pH analysis showed that the coarse-mode aerosol
436 pH was approximately equal to or even higher than 7 for all three seasons, which was considerably
437 higher than the pH of fine particles. The presence of Ca^{2+} and Mg^{2+} had a crucial effect on coarse-
438 mode aerosol pH. Under heavily polluted conditions, the mass fractions of Ca^{2+} and Mg^{2+} in coarse
439 particles decreased significantly, resulting in an evident increase in the acidity of the coarse particles.
440 The $\text{PM}_{2.5}$ pH sensitivity tests also showed that when evaluating aerosol acidity, the role of crustal
441 ions cannot be ignored in areas or seasons (such as spring) where mineral dust is an important
442 particle source. In northern China, dust can effectively buffer acidity in aerosols or precipitation.

443 The sensitivity tests in this work showed that the common important driving factors affecting
444 $\text{PM}_{2.5}$ pH are SO_4^{2-} , TNH_3 , and T, while unique influencing factors were Ca^{2+} in spring and RH in
445 summer. In recent years, NO_3^- has generally dominated the inorganic ions in the NCP. However,
446 owing to the significantly rich ammonia content in the atmosphere in spring and summer, the $\text{PM}_{2.5}$
447 pH in only winter and autumn decreased obviously with elevated TNO_3 . Excess NH_3 in the
448 atmosphere and a high NO_3^- mass fraction in $\text{PM}_{2.5}$ may be the reason why aerosol acidity in China
449 is lower than that in Europe and the United States. Notably, TNH_3 had a great influence on aerosol

450 acidity at lower concentrations but had a limited influence on $PM_{2.5}$ pH when present in excess. The
451 nonlinear relationship between $PM_{2.5}$ pH and TNH_3 indicated that although NH_3 in the NCP was
452 abundant, the $PM_{2.5}$ pH was still acidic, which might be attributed to the limited ALWC and the
453 hydrolysis of ammonium salts.

454 In addition to the particle chemical compositions, meteorological conditions also had important
455 impacts on aerosol acidity. When the mass concentration of water-soluble matter was higher, such
456 as during severe haze events in winter, the higher RH clearly increased aerosol acidity. An opposite
457 tendency was observed when the mass concentration of water-soluble matter was low, such as in
458 summer: the dilution effect of ALWC on H_{air}^+ was more obvious. At higher ambient temperatures,
459 more ammonium nitrate and ammonium chloride volatilized, while ALWC decreased, which could
460 further reduce the $PM_{2.5}$ pH.

461 In recent years, nitrates have dominated $PM_{2.5}$ in the NCP, especially on heavily polluted days.
462 Sensitivity tests showed that decreasing TNO_3 could lower $\epsilon(NH_4^+)$ and that decreasing TNH_3 could
463 also lower $\epsilon(NO_3^-)$, helping to reduce nitrate production. However, the $\epsilon(NO_3^-)$ response to TNH_3
464 control was highly nonlinear. Given that ammonia was excessive in most cases, a decrease in nitrate
465 would occur only if TNH_3 were greatly reduced. Therefore, in terms of controlling the generation
466 of nitrate, a reduction in NO_x emissions is more feasible than a reduction in NH_3 emissions.

467

468 *Data availability.* All data in this work are available by contacting the corresponding author P. S.
469 Zhao (pszhao@ium.cn).

470

471 *Author contributions.* P Z designed and led this study. J D and P Z interpreted the data and discussed
472 the results. J S and X D analysed the chemical compositions of size-resolved aerosol samples. J D
473 and P Z wrote the manuscript.

474

475 *Competing interests.* The authors declare that they have no conflict of interest.

476

477 *Acknowledgements.* This work was supported by the National Natural Science Foundation of China
478 (41675131), the Beijing Talents Fund (2014000021223ZK49), and the Beijing Natural Science
479 Foundation (8131003). Special thanks are extended to the Max Planck Institute for Chemistry and
480 Leibniz Institute for Tropospheric Research where Dr. Zhao visited as a guest scientist in 2018.

481 **References**

482 Bian, Y. X., Zhao, C. S., Ma, N., Chen, J., Xu, W. Y.: A study of aerosol liquid water content based
483 on hygroscopicity measurements at high relative humidity in the North China Plain. *Atmos. Chem.*
484 *Phys.* 14, 6417-6426, 2014.

485 Bougiatioti, A., Nikolaou, P., Stavroulas, I., Kouvarakis, G., Weber, R., Nenes, A., Kanakidou, M.,
486 Mihalopoulos, N.: Particle water and pH in the eastern Mediterranean: Source variability and
487 implications for nutrient availability, *Atmos. Chem. Phys.*, 16(7), 4579-4591, 2016.

488 Chen, X., Walker, J. T., and Geron, C.: Chromatography related performance of the Monitor for
489 AeRosols and GAses in ambient air (MARGA): laboratory and field-based evaluation, *Atmos.*
490 *Meas. Tech.*, 10, 3893-3908, 2017.

491 Cheng, Y. F., Zheng, G. J., Wei C., Mu, Q., Zheng, B., Wang, Z. B., Gao, M., Zhang, Q., He, K. B.,
492 Carmichael, G., Pöschl, U., Su, H.: Reactive nitrogen chemistry in aerosol water as a source of
493 sulfate during haze events in China, *Sci. Adv.*, 2:e1601530, 2016.

494 Chi, X. Y., P. Z. He, Z. Jiang, et al.: Acidity of aerosols during winter heavy haze events in Beijing
495 and Gucheng, China. *J. Meteor. Res.*, 32, 14–25, 2018.

496 Clegg, S. L., et al.: A thermodynamic model of the system H^+ , NH_4^+ , SO_4^{2-} , NO_3^- , H_2O at
497 tropospheric temperatures, *J. Phys. Chem. 102A*, 2137-2154, 1998.

498 Cruz, C. N., Dassios, K. G., Pandis, S. N.: The effect of dioctyl phthalate films on the ammonium
499 nitrate aerosol evaporation rate. *Atmos. Environ.*, 34, 3897-3905, 2000.

500 Dassios, K. G., Pandis, S. N.: The mass accommodation coefficient of ammonium nitrate aerosol.
501 *Atmos. Environ.*, 33 (18), 2993-3003, 1999.

502 Ding, J., Zhang, Y. F., Han, S. Q., Xiao, Z. M., Wang, J., and Feng, Y. C.: Chemical, optical and
503 radiative characteristics of aerosols during haze episodes of winter in the North China Plain,
504 *Atmos. Environ.*, 181, 164-176, 2018.

505 Ding, X. X., Kong, L. D., Du, C. T., Zhanzakova, A., Fu, H. B., Tang, X. F., Wang, L., Yang, X.,
506 Chen, J. M., and Cheng, T. T.: Characteristics of size-resolved atmospheric inorganic and
507 carbonaceous aerosols in urban Shanghai, *Atmos. Environ.*, 167, 625-641, 2017.

508 Eddingsaas, N. C., VanderVelde, D. G., and Wennberg, P. O.: Kinetics and products of the acid-
509 catalyzed ring-opening of atmospherically relevant butyl epoxy alcohols, *J. Phys. Chem. A*, 114,
510 8106-8113, 2010.

511 Engelhart, G. J., Hildebrandt, L., Kostenidou, E., Mihalopoulos, N., Donahue, N. M., and Pandis,
512 S. N.: Water content of aged aerosol, *Atmos. Chem. Phys.*, 11, 911-920, 2011.

513 Fang, T., Guo, H. Y., Zeng, L. H., Verma, V., Nenes, A., Weber, R. J.: Highly acidic ambient particles,
514 soluble metals, and oxidative potential: A link between sulfate and aerosol toxicity, *Environ. Sci.*
515 *Technol.*, 51, 2611-2620, 2017.

516 Fountoukis, C., and Nenes, A.: ISORROPIA II A computationally efficient aerosol thermodynamic
517 equilibrium model for K^+ , Ca^{2+} , Mg^{2+} , NH_4^+ , Na^+ , SO_4^{2-} , NO_3^- , Cl^- , H_2O aerosols, *Atmos. Chem.*
518 *Phys.* 7, 4639-4659, 2007.

519 Fountoukis, C., Nenes, A., Sullivan, A., Weber, R., Van Reken, T., Fischer, M., Matías, E., Moya,
520 M., Farmer, D., and Cohen, R. C.: Thermodynamic characterization of Mexico City aerosol
521 during MILAGRO 2006, *Atmos. Chem. Phys.*, 9, 2141-2156, 2009.

522 Fu, X., Guo, H., Wang, X., Ding, X., He, Q., Liu, T., and Zhang, Z.: $PM_{2.5}$ acidity at a background
523 site in the Pearl River Delta region in fall-winter of 2007-2012, *J Hazard Mater*, 286, 484-492,
524 2015.

525 Gao, J. J., Wang, K., Wang, Y., Liu, S. H., Zhu, C. Y., Hao, J. M., Liu, H. J., Hua, S. B., Tian, H. Z.:

526 Temporal-spatial characteristics and source apportionment of PM_{2.5} as well as its associated
527 chemical species in the Beijing-Tianjin-Hebei region of China. *Environ. Pollut.*, 233, 714-724,
528 2018.

529 Galon-Negru, A. G., Olariu, R. I., and Arsene, C.: Chemical characteristics of size-resolved
530 atmospheric aerosols in Iasi, north-eastern Romania: nitrogen-containing inorganic compounds
531 control aerosol chemistry in the area, *Atmos. Chem. Phys.*, 18, 5879-5904, 2018.

532 Guo, H., Sullivan, A. P., Campuzano-Jost, P., Schroder, J. C., Lopez-Hilfiker, F. D., Dibb, J. E.,
533 Jimenez, J. L., Thornton, J. A., Brown, S. S., Nenes, A., Weber, R. J.: Fine particle pH and the
534 partitioning of nitric acid during winter in the northeastern United States, *J. Geophys. Res. Atmos.*,
535 121, 10355-10376, 2016.

536 Guo, H., Xu, L., Bougiatioti, A., Cerully, K. M., Capps, S. L., Hite Jr., J. R., Carlton, A. G., Lee, S.-
537 H., Bergin, M. H., Ng, N. L., Nenes, A., Weber, R. J.: Fine-particle water and pH in the
538 southeastern United States, *Atmos. Chem. Phys.*, 15, 5211-5228, 2015.

539 Guo, H., Weber, R. J., and Nenes, A.: High levels of ammonia do not raise fine particle pH
540 sufficiently to yield nitrogen oxide-dominated sulfate production, *Sci. Rep.*, 7, doi:
541 10.1038/s41598-017-11704-0, 2017.

542 Guo, H. Y., Otjes, R., Schlag, P., Kiendler-Scharr, A., Nenes, A., and Weber, R. J.: Effectiveness of
543 ammonia reduction on control of fine particle nitrate, *Atmos. Chem. Phys.*, 18, 12241-12256,
544 2018.

545 Hennigan, C. J., Izumi, J., Sullivan, A. P., Weber, R. J., and Nenes, A.: A critical evaluation of proxy
546 methods used to estimate the acidity of atmospheric particles, *Atmos. Chem. Phys.*, 15, 2775-
547 2790, 2015.

548 Huang, X. J., Liu, Z. R., Liu, J. Y., Hu, B., Wen, T. X., Tang, G. Q., Zhang, J. K., Wu, F. K., Ji, D.
549 S., Wang, L. L., Wang, Y. S.: Chemical characterization and source identification of PM_{2.5} at
550 multiple sites in the Beijing–Tianjin–Hebei region, China, *Atmos. Chem. Phys.*, 17, 12941–12962,
551 2017.

552 Liu, M. X., Song, Y., Zhou, T., Xu, Z. Y., Yan, C. Q., Zheng, M., Wu, Z. J., Hu, M., Wu, Y. S., and
553 Zhu, T.: Fine particle pH during severe haze episodes in northern China, *Geophys. Res. Lett.*,
554 44, 5213-5221, 2017.

555 Ma, Q.X., Wu, Y.F., Zhang, D. Z., Wang, X.J., Xia, Y.J., Liu, X.Y., Tian, P., Han, Z.W., Xia, X.G.,
556 Wang, Y., Zhang, R.J.: Roles of regional transport and heterogeneous reactions in the PM_{2.5}
557 increase during winter haze episodes in Beijing, *Sci. Total Environ.*, 599-600, 246-253, 2017.

558 Meier, J., Wehner, B., Massling, A., Birmili, W., Nowak, A., Gnauk, T., Brüggemann, E., Herrmann,
559 H., Min, H., Wiedensohler, A.: Hygroscopic growth of urban aerosol particles in Beijing (China)
560 during wintertime: a comparison of three experimental methods, *Atmos. Chem. Phys.*, 9, 6865–
561 6880, 2009.

562 Meskhidze, N., Chameides, W. L., Nenes, A., and Chen, G.: Iron mobilization in mineral dust: Can
563 anthropogenic SO₂ emissions affect ocean productivity? *Geophys. Res. Lett.*, 30, 2085,

564 doi:10.1029/2003gl018035, 2003.

565 Nenes, A., Pandis, S. N., and Pilinis, C.: ISORROPIA: A new thermodynamic equilibrium model
566 for multiphase multicomponent inorganic aerosols, *Aquat Geochem*, 4, 123-152, 1998.

567 Nowak, J. B., Huey, L. G., Russell, A. G., Tian, D., Neuman, J. A., Orsini, D., Sjostedt, S. J., Sullivan,
568 A. P., Tanner, D. J., Weber, R. J., Nenes, A., Edgerton, E., Fehsenfeld, F. C.: Analysis of urban
569 gas phase ammonia measurements from the 2002 Atlanta Aerosol Nucleation and Real-Time
570 Characterization Experiment (ANARChE), *J. Geophys. Res.*, 111, D17308,
571 doi:10.1029/2006jd007113, 2006.

572 Pan, X. L., Yan, P., Tang, J., Ma, J. Z., Wang, Z. F., Gbaguidi, A., and Sun, Y. L.: Observational
573 study of influence of aerosol hygroscopic growth on scattering coefficient over rural area near
574 Beijing mega-city, *Atmos. Chem. Phys.*, 9, 7519-7530, 2009.

575 Pathak, R. K., Wang, T., Ho, K. F., Lee, S. C.: Characteristics of summertime PM_{2.5} organic and
576 elemental carbon in four major Chinese cities: Implications of high acidity for water soluble
577 organic carbon (WSOC), *Atmos. Environ.*, 45, 318-325, 2011a.

578 Pathak, R. K., Wang, T. and Wu, W.S.: Nighttime enhancement of PM_{2.5} nitrate in ammonia-poor
579 atmospheric conditions in Beijing and Shanghai: Plausible contributions of heterogeneous
580 hydrolysis of N₂O₅ and HNO₃ partitioning. *Atmos. Environ.*, 45: 1183-1191, 2011b.

581 Peng, C. G., Chan, M. N., and Chan, C. K.: The hygroscopic properties of dicarboxylic and
582 multifunctional acids: Measurements and UNIFAC predictions, *Environ. Sci. Technol.*, 35, 4495-
583 4501, 2001.

584 Rengarajan, R., Sudheer, A.K., Sarin, M.M.: Aerosol acidity and secondary formation during
585 wintertime over urban environment in western India. *Atmos. Environ.*, 45: 1940-1945, 2011.

586 Rumsey, I. C., Cowen, K. A., Walker, J. T., Kelly, T. J., Hanft, E. A., Mishoe, K., Rogers, C., Proost,
587 R., Beachley, G. M., Lear, G., Frelink, T., and Otjes, R. P.: An assessment of the performance of
588 the Monitor for AeRosols and GAses in ambient air (MARGA): a semi-continuous method for
589 soluble compounds, *Atmos. Chem. Phys.*, 14, 5639-5658, 2014.

590 Schwertmann, U., Cornell, R. M.: *Iron Oxides In the Laboratory: Preparation and Characterization*,
591 Weinheim, WCH Publisher, 1991.

592 Seinfeld, J. H., Pandis, S. N.: *Atmospheric Chemistry and Physics: From Air Pollution to Climate*
593 *Change*, John Wiley & Sons, Inc., Hoboken, New Jersey, USA, 2016.

594 Shi, G. L., Xu, J., Peng, X., Xiao, Z. M., Chen, K., Tian, Y. Z., Guan, X. P., Feng, Y. C., Yu, H. F.,
595 Nenes, A., Russell, A. G.: pH of aerosols in a polluted atmosphere: source contributions to highly
596 acidic aerosol, *Environ. Sci. Technol.*, DOI: 10.1021/acs.est.6b05736, 2017.

597 Shi, Z., Bonneville, S., Krom, M. D., Carslaw, K. S., Jickells, T. D., Baker, A. R., Benning, L. G.:
598 Iron dissolution kinetics of mineral dust at low pH during simulated atmospheric processing.
599 *Atmos. Chem. Phys.*, 11, 995-1007, 2011.

600 Song, S. J., Gao, M., Xu, W. Q., Shao, J. Y., Shi, G. L., Wang, S. X., Wang, Y. X., Sun, Y. L., McElroy,
601 M. B.: Fine particle pH for Beijing winter haze as inferred from different thermodynamic

602 equilibrium models. *Atmos. Chem. Phys.*, 18, 7423-7438, 2018.

603 Su, J., Zhao, P. S., Dong, Q.: Chemical Compositions and Liquid Water Content of Size-Resolved
604 Aerosol in Beijing. *Aerosol Air Qual. Res.*, 18, 680-692, 2018.

605 Surratt, J. D., Chan, A. W., Eddingsaas, N. C., Chan, M., Loza, C. L., Kwan, A. J., Hersey, S. P.,
606 Flagan, R. C., Wennberg, P. O., and Seinfeld, J. H.: Reactive intermediates revealed in secondary
607 organic aerosol formation from isoprene, *PNAS. USA*, 107, 6640-6645, 2010.

608 Tan, T. Y., Hu, M., Li, M. R., Guo, Q. F., Wu, Y. S., Fang, X., Gu, F. T., Wang, Y., Wu, Z. J.: New
609 insight into PM_{2.5} pollution patterns in Beijing based on one-year measurement of chemical
610 compositions. *Sci. Total Environ.*, 621, 734-743, 2018.

611 Tian, S. L., Pan, Y. P., Liu, Z.R., Wen, T. X., Wang, Y. S.: Size-resolved aerosol chemical analysis
612 of extreme haze pollution events during early 2013 in urban Beijing, China. *J. Hazard. Mater.*,
613 279, 452-460, 2014.

614 Wang, G., Zhang, R., Gomez, M. E., Yang, L., Levy Zamora, M., Hu, M., Lin, Y., Peng, J., Guo, S.,
615 Meng, J., Li, J., Cheng, C., Hu, T., Ren, Y., Wang, Y., Gao, J., Cao, J., An, Z., Zhou, W., Li, G.,
616 Wang, J., Tian, P., Marrero-Ortiz, W., Secrest, J., Du, Z., Zheng, J., Shang, D., Zeng, L., Shao,
617 M., Wang, W., Huang, Y., Wang, Y., Zhu, Y., Li, Y., Hu, J., Pan, B., Cai, L., Cheng, Y., Ji, Y.,
618 Zhang, F., Rosenfeld, D., Liss, P. S., Duce, R. A., Kolb, C. E., and Molina, M. J.: Persistent sulfate
619 formation from London Fog to Chinese haze, *Proc. Natl. Acad. Sci. U.S.A.*, 113, 13630-13635,
620 2016.

621 Wang, X. W., Jing, B., Tan, F., Ma, J.B., Zhang, Y. H., Ge, M.F.: Hygroscopic behavior and chemical
622 composition evolution of internally mixed aerosols composed of oxalic acid and ammonium
623 sulfate, *Atmos. Chem. Phys.*, 17, 12797-12812, 2017.

624 Weber, R. J., Guo, H., Russell, A. G., Nenes, A.: High aerosol acidity despite declining atmospheric
625 sulfate concentrations over the past 15 years. *Nat. Geosci.*, 9, 282-285, 2016.

626 Young, A. H., Keene, W. C., Pszenny, A. A. P., Sander, R., Thornton, J. A., Riedel, T. P., Maben, J.
627 R.: Phase partitioning of soluble trace gases with size-resolved aerosols in near-surface
628 continental air over northern Colorado, USA, during winter, *J. Geophys. Res. Atmos.*, 118, 9414-
629 9427, doi:10.1002/jgrd.50655, 2013.

630 Zhang, Q., Jimenez, J. L., Worsnop, D. R., Canagaratna, M.: A case study of urban particle acidity
631 and its influence on secondary organic aerosol. *Environ. Sci. Technol.*, 41, 3213-3219, 2007.

632 Zhang, H., Cheng, S., Li, J., Yao, S., and Wang, X.: Investigating the aerosol mass and chemical
633 components characteristics and feedback effects on the meteorological factors in the Beijing-
634 Tianjin-Hebei region, China, *Environ Pollut*, 244, 495-50, 2019.

635 Zhang, Y., Lang, J., Cheng, S., Li, S., Zhou, Y., Chen, D., Zhang, H., and Wang, H.: Chemical
636 composition and sources of PM₁ and PM_{2.5} in Beijing in autumn, *Sci Total Environ*, 630, 72-82,
637 2018.

638 Zhao, P. S., Chen, Y. N., Su, J.: Size-resolved carbonaceous components and water-soluble ions
639 measurements of ambient aerosol in Beijing. *J. Environ. Sci.*, 54, 298-313, 2017.

640 Zhao, P. S., Dong, F., He, D., Zhao, X.J., Zhang, X.L., Zhang, W.Z., Yao, Q., Liu, H. Y.:
641 Characteristics of concentrations and chemical compositions for PM_{2.5} in the region of Beijing,
642 Tianjin, and Hebei, China. *Atmos. Chem. Phys.*, 13, 4631-4644, 2013.

643 Zou, J. N., Liu, Z. R., Hu, B., Huang, X. J., Wen, T. X., Ji, D. S., Liu, J. Y., Yang, Y., Yao, Q., Wang,
644 Y. S.: Aerosol chemical compositions in the North China Plain and the impact on the visibility in
645 Beijing and Tianjin. *Atmos. Res.* 201, 235-246, 2018.

646 **Table captions**

647 **Table 1.** Average mass concentrations of NO_3^- , SO_4^{2-} , NH_4^+ and $\text{PM}_{2.5}$, as well as ALWC, H_{air}^+ , and
648 $\text{PM}_{2.5}$ pH, under clean, polluted, and heavily polluted conditions over four seasons.

649 **Table 2.** Sensitivity of $\text{PM}_{2.5}$ pH to SO_4^{2-} , TNH_3 , TNO_3 , Ca^{2+} , RH, and T. A larger magnitude of the
650 relative standard deviation (RSD) represents a larger impact derived from variations in variables.

651 **Table 3.** Average measured $\varepsilon(\text{NH}_4^+)$, $\varepsilon(\text{NO}_3^-)$, and $\varepsilon(\text{Cl}^-)$ based on the real-time MARGA dataset
652 and ambient temperature at different ambient RH levels in four seasons.

653

654

655

Table 1

Spring	PM _{2.5}	NO ₃ ⁻	SO ₄ ²⁻	NH ₄ ⁺	ALWC*	H _{air} ⁺ *	pH*
	µg m ⁻³	µg m ⁻³	µg m ⁻³	µg m ⁻³	µg m ⁻³	µg m ⁻³	
Average	57±42	12.6±14.2	8.4±7.7	6.7±7.2	21±33	3.7E-06±1.5E-05	4.4±1.2
Clean	39±19	6.6±6.5	5.4±3.8	3.6±3.2	13±23	3.2E-06±1.9E-05	4.6±1.4
Polluted	101±21	30.7±14.3	16.2±6.2	15.3±6.0	33±36	3.1E-06±2.9E-06	4.1±0.4
Heavily polluted	199±62	36.4±19.8	29.3±14.0	23.2±12.3	78±60	1.6E-05±5.4E-06	3.7±0.3
Winter	PM _{2.5}	NO ₃ ⁻	SO ₄ ²⁻	NH ₄ ⁺	ALWC*	H _{air} ⁺ *	pH*
Average	60±69	13.7±21.0	7.3±8.7	7.3±10.0	35±46	2.2E-05±2.3E-04	4.5±0.7
Clean	22±20	3.6±3.9	2.8±1.8	2.2±2.0	10±16	3.2E-07±4.8E-07	4.5±0.6
Polluted	107±21	18.9±8.6	11.0±5.7	11.0±4.7	41±45	1.9E-05±9.1E-05	4.8±1.0
Heavily polluted	209±39	59.7±21.8	26.2±6.3	29.1±8.7	80±52	7.0E-05±4.7E-04	4.4±0.7
Summer	PM _{2.5}	NO ₃ ⁻	SO ₄ ²⁻	NH ₄ ⁺	ALWC*	H _{air} ⁺ *	pH*
Average	39±24	9.5±9.5	8.6±7.5	7.2±5.6	50±68	1.6E-05±1.8E-05	3.8±1.2
Clean	33±18	7.3±6.8	7.0±6.0	5.9±4.0	42±61	1.4E-05±1.6E-05	3.8±1.2
Polluted	87±13	26.5±10.5	20.7±7.0	17.6±4.8	100±88	3.1E-05±2.0E-05	3.5±0.4
Autumn	PM _{2.5}	NO ₃ ⁻	SO ₄ ²⁻	NH ₄ ⁺	ALWC*	H _{air} ⁺ *	pH*
Average	59±48	18.5±19.5	6.5±5.9	8.2±8.2	109±160	8.1E-06±1.1E-05	4.3±0.8
Clean	33±21	7.6±7.4	4.4±4.1	3.8±3.5	49±83	3.8E-06±6.6E-06	4.5±1.0
Polluted	105±21	33.8±11.6	14.3±6.3	16.0±4.6	225±189	1.7E-05±1.2E-05	4.1±0.3
Heavily polluted	174±18	63.4±15.4	25.0±15.9	29.0±5.1	317±236	2.2E-05±1.0E-05	4.1±0.2

656

* For data with RH>30%.

657

658

Table 2

Impact Factor	SO ₄ ²⁻	TNO ₃	TNH ₃	Ca ²⁺	RH	T
Spring- RSD	12.4%	5.2%	3.9%	7.5%	1.3%	7.0%
Winter- RSD	28.1%	8.4%	27.0%	1.0%	4.1%	6.7%
Summer- RSD	7.9%	3.6%	8.1%	1.9%	8.6%	5.8%
Autumn- RSD	6.0%	3.3%	16.1%	0.8%	2.4%	7.5%

659

660

661

662

Table 3

	RH	T, °C	$\varepsilon(\text{NH}_4^+)$	$\varepsilon(\text{NO}_3^-)$	$\varepsilon(\text{Cl}^-)$
Spring	$\leq 30\%$	24.8 ± 3.7	0.17 ± 0.14	0.84 ± 0.12	0.67 ± 0.24
	30~60%	20.6 ± 3.8	0.25 ± 0.14	0.91 ± 0.06	0.82 ± 0.16
	$>60\%$	15.8 ± 2.7	0.28 ± 0.12	0.96 ± 0.03	0.96 ± 0.06
Winter	$\leq 30\%$	5.4 ± 5.3	0.31 ± 0.13	0.78 ± 0.12	0.89 ± 0.14
	30~60%	1.0 ± 3.6	0.50 ± 0.21	0.89 ± 0.10	0.97 ± 0.03
	$>60\%$	-1.9 ± 2.1	0.60 ± 0.20	0.96 ± 0.03	0.99 ± 0.01
Summer	$\leq 30\%$	35.6 ± 0.4	0.06 ± 0.02	0.35 ± 0.20	0.39 ± 0.17
	30~60%	29.6 ± 4.2	0.17 ± 0.11	0.65 ± 0.23	0.43 ± 0.16
	$>60\%$	25.2 ± 3.8	0.26 ± 0.12	0.90 ± 0.12	0.71 ± 0.15
Autumn	$\leq 30\%$	21.7 ± 7.5	0.07 ± 0.06	0.49 ± 0.25	0.45 ± 0.21
	30~60%	20.8 ± 6.3	0.21 ± 0.14	0.82 ± 0.19	0.67 ± 0.21
	$>60\%$	14.9 ± 5.7	0.30 ± 0.19	0.92 ± 0.10	0.86 ± 0.13

663

664

665

666 **Figure captions**

667 **Figure 1.** Time series of relative humidity (RH) and temperature (T) (a, e, i, m); PM_{2.5}, PM₁₀, and
668 NH₃ (b, f, g, n); dominant water-soluble ions: NO₃⁻, SO₄²⁻, and NH₄⁺ (c, g, k, o); and PM_{2.5} pH
669 coloured by PM_{2.5} concentration (d, h, l, p) over four seasons.

670 **Figure 2.** Comparisons of predicted and measured NH₃, HNO₃, HCl, NH₄⁺, NO₃⁻, Cl⁻, ε(NH₄⁺),
671 ε(NO₃⁻), and ε(Cl⁻) coloured by RH. In this figure, the data from all four seasons were combined;
672 comparisons of individual seasons are shown in Figure S1-S4.

673 **Figure 3.** Comparisons of predicted and iterative NH₃, HNO₃, and HCl, as well as predicted and
674 measured NH₄⁺, NO₃⁻, Cl⁻, ε(NH₄⁺), ε(NO₃⁻), and ε(Cl⁻) coloured by particle size. In this figure, all
675 MOUDI data were combined.

676 **Figure 4.** Time series of mass fractions of NO₃⁻, SO₄²⁻, NH₄⁺, Cl⁻, Mg²⁺, and Ca²⁺ with respect to
677 the total ion content, as well as PM_{2.5} pH in all four seasons (PM_{2.5} pH values at RH≤30% were
678 excluded).

679 **Figure 5.** Wind-dependence map of PM_{2.5} pH over four seasons. In each picture, the shaded contour
680 indicates the mean value of PM_{2.5} pH for varying wind speeds (radial direction) and wind directions
681 (transverse direction) (data at RH≤30% were excluded).

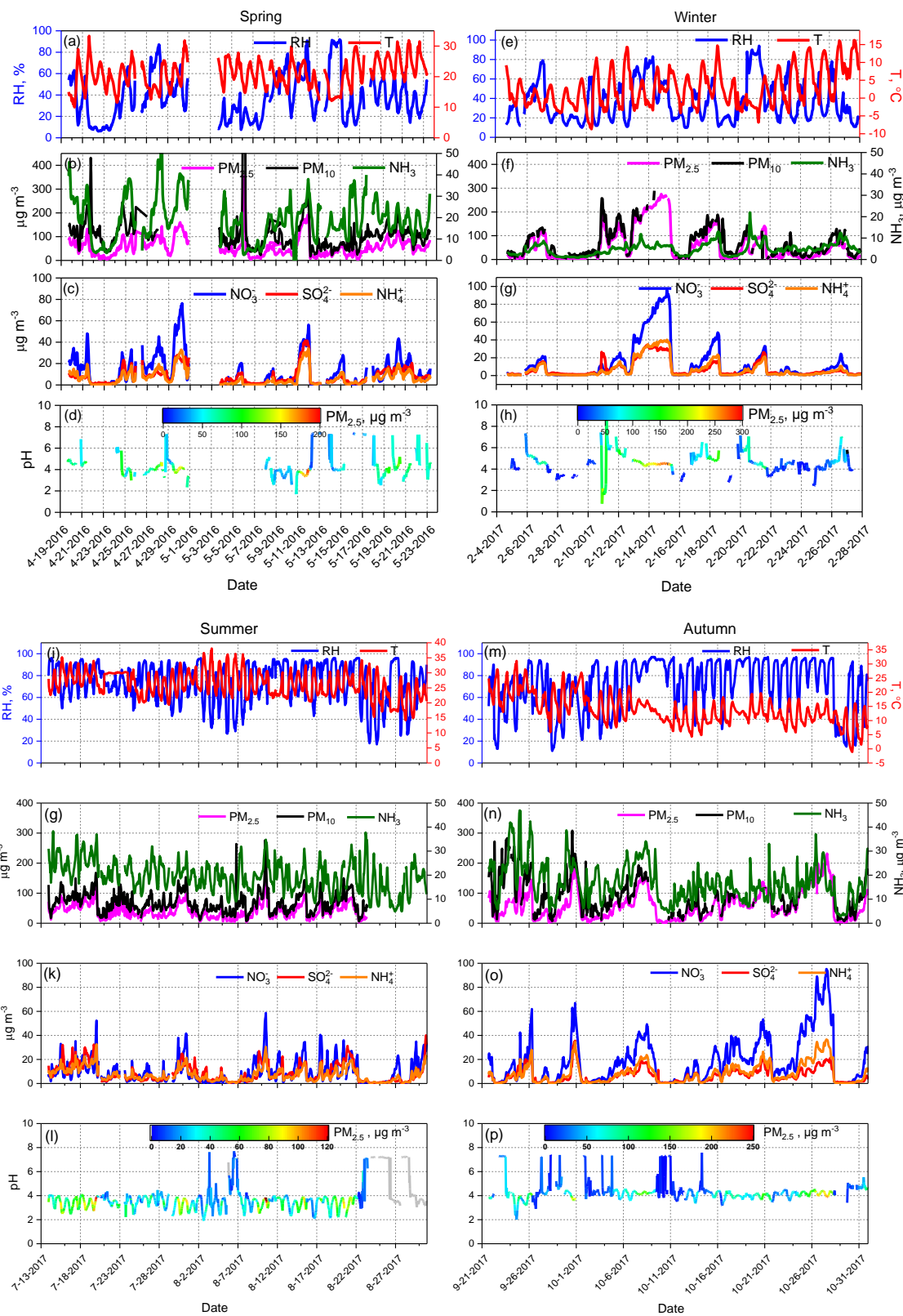
682 **Figure 6.** Diurnal patterns of mass concentrations of NO₃⁻ and SO₄²⁻ in PM_{2.5}, predicted aerosol
683 liquid water content (ALWC), H_{air}⁺, and PM_{2.5} pH over four seasons. Mean and median values are
684 shown, together with 25% and 75% quantiles. Data at RH≤30% were excluded, and the shaded area
685 represents the time period when most RH values were lower than 30%.

686 **Figure 7.** Sensitivity tests of PM_{2.5} pH to SO₄²⁻, TNO₃, TNH₃, Ca²⁺, and meteorological parameters
687 (RH and T) in summer (S) and winter (W).

688 **Figure 8.** Sensitivity tests of ε(NH₄⁺), ε(NO₃⁻) to TNO₃, TNH₃, RH and T coloured by PM_{2.5} pH in
689 summer (S) and winter (W).

690 **Figure 9.** Size distributions of aerosol pH and all analysed chemical components under clean (a, d,
691 g), polluted (b, e, h), and heavily polluted conditions (c, f, i) in summer, autumn, and winter.

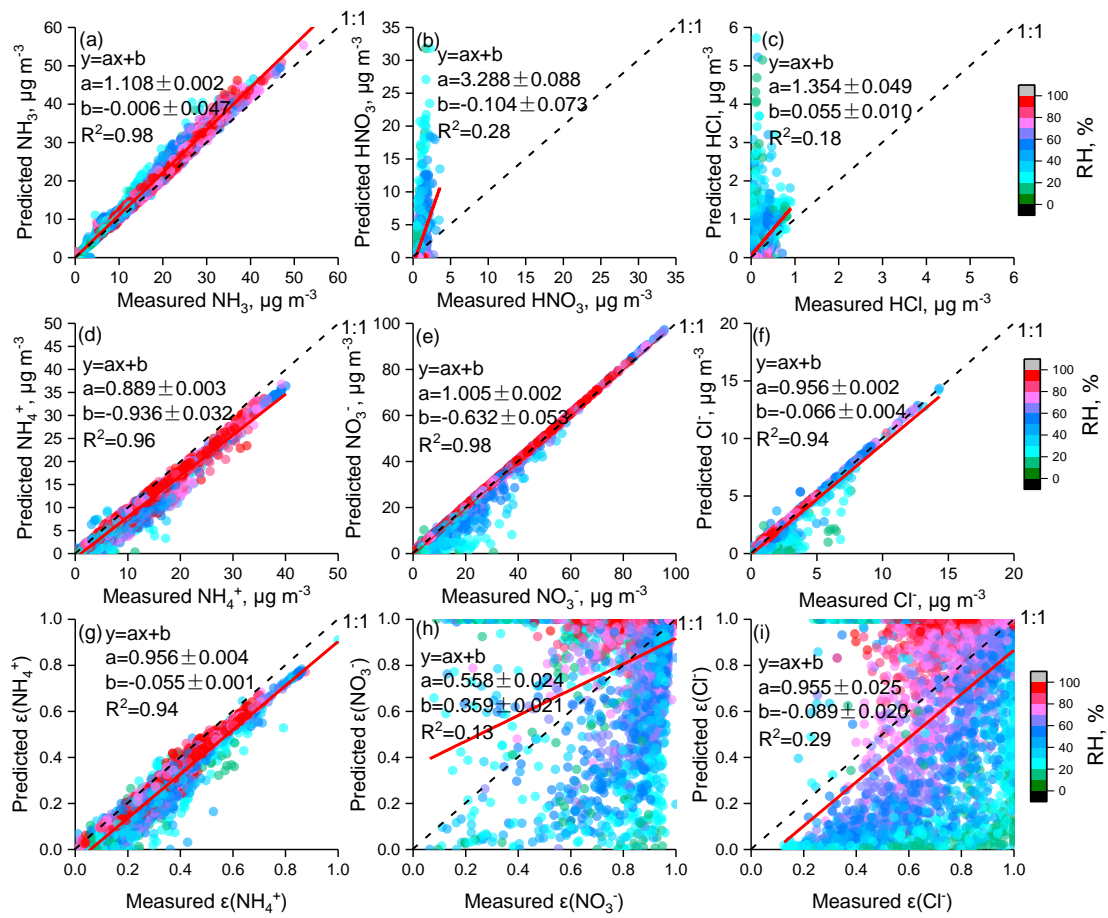
692



693

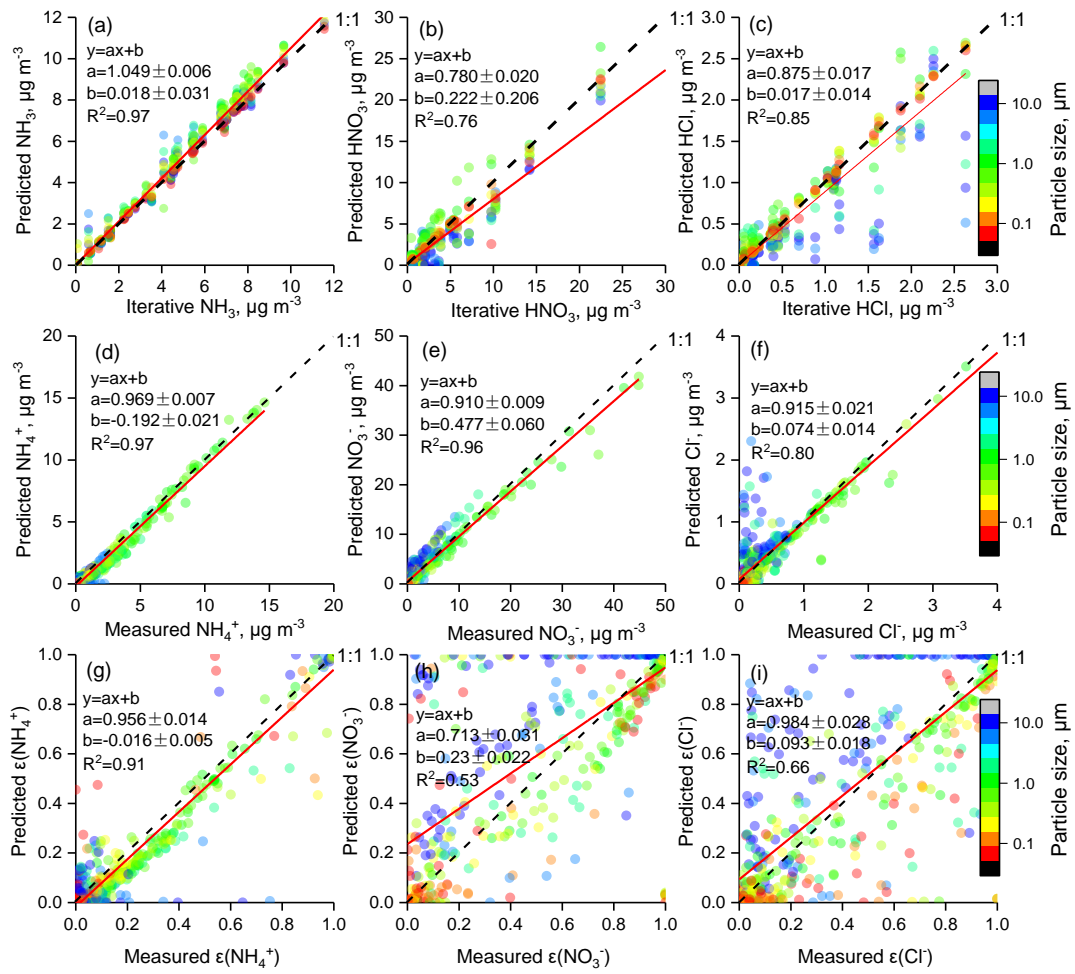
694
695

Figure 1.



696
697
698

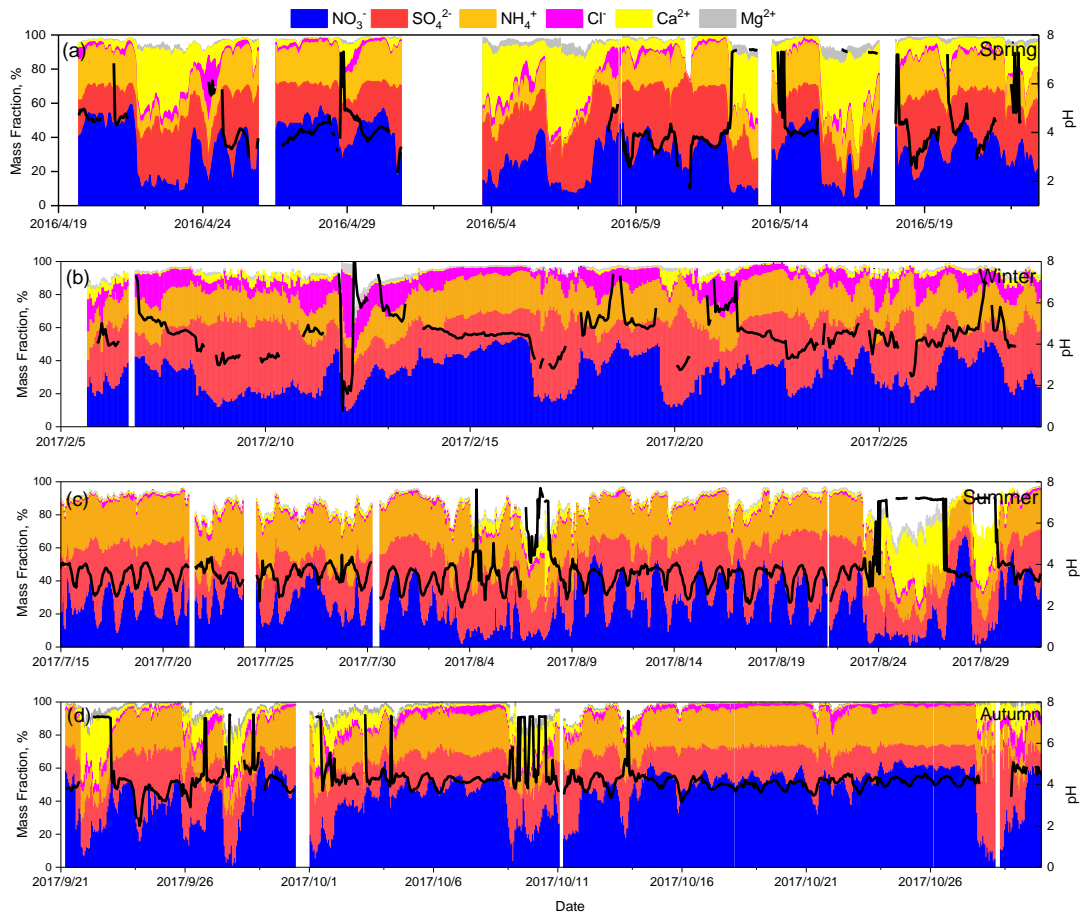
Figure 2.



699

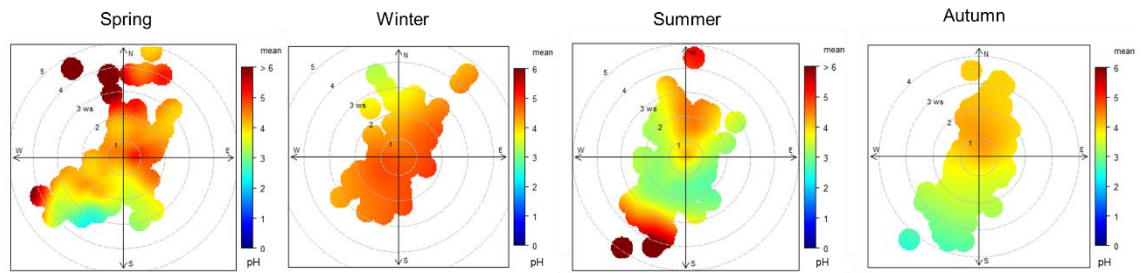
700

Figure 3.



701
702
703

Figure 4.



704
705
706
707
708

Figure 5.

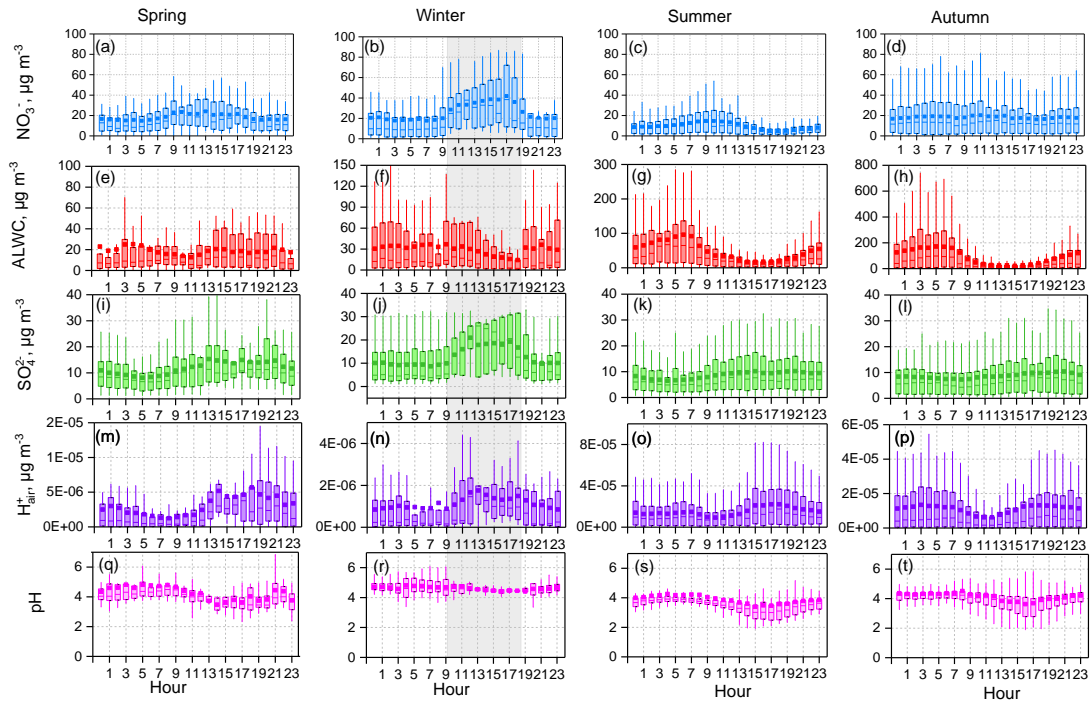


Figure 6.

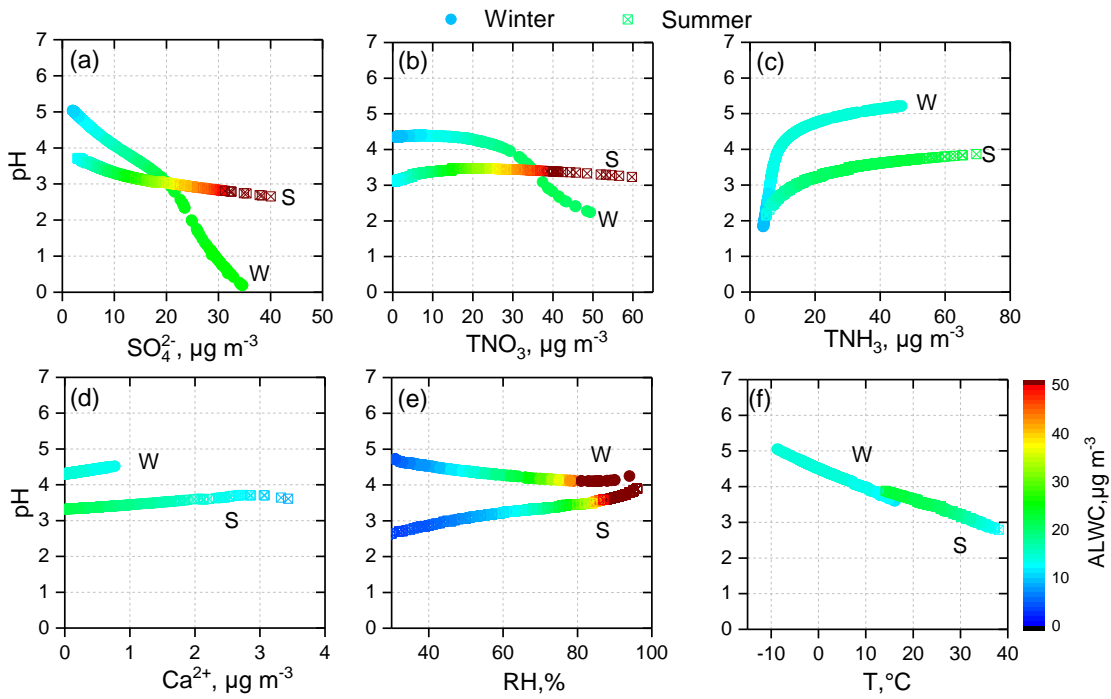


Figure 7.

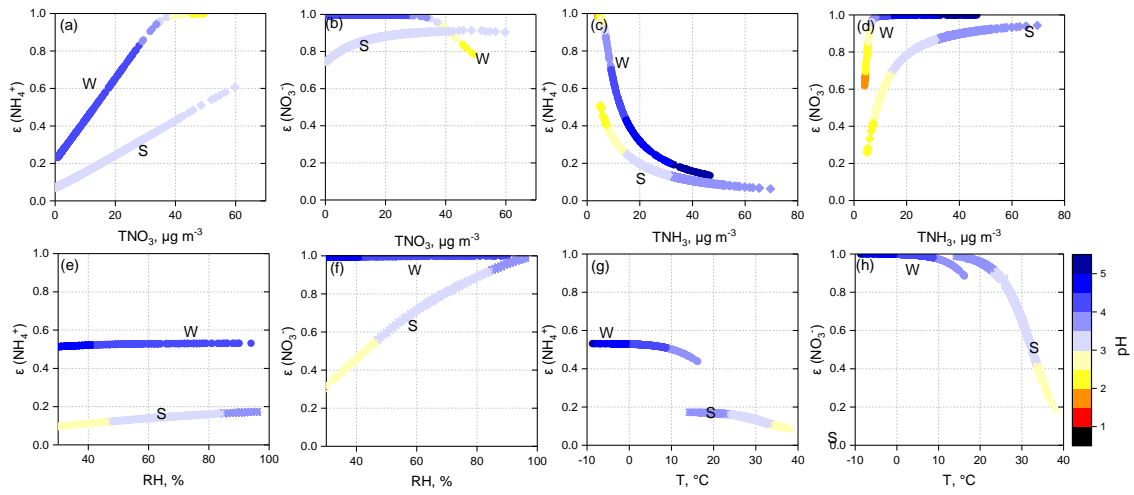
709

710

711

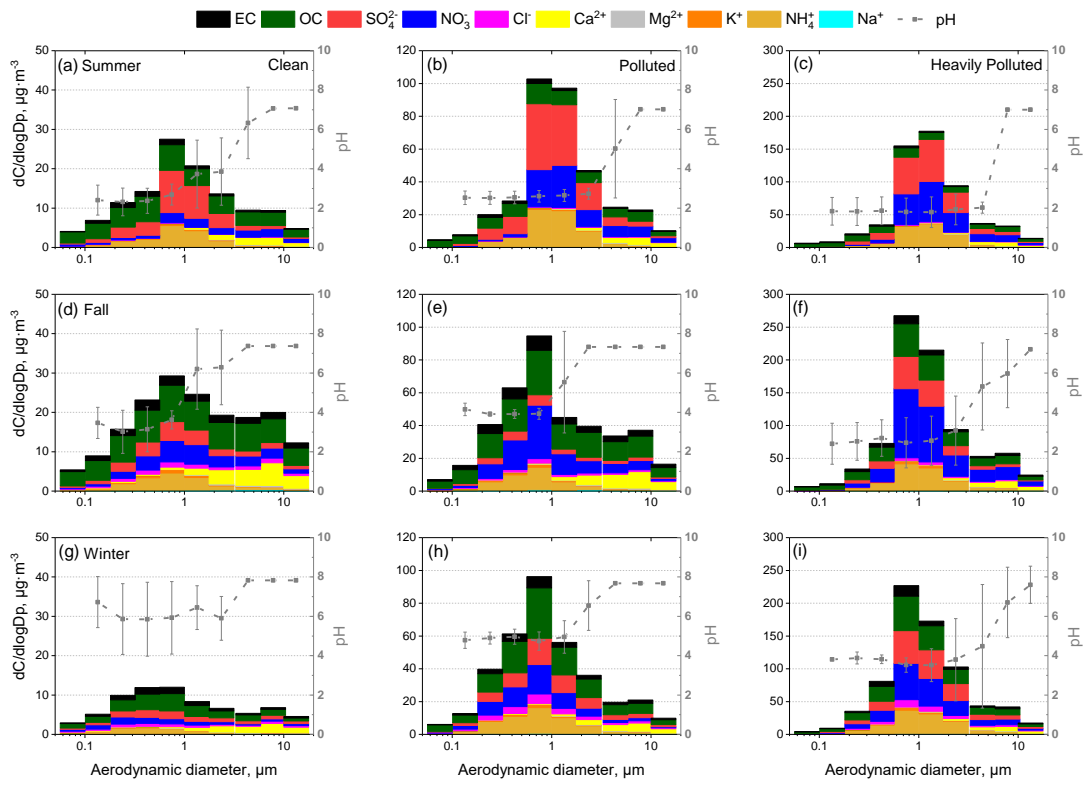
712

713



714
715
716
717

Figure 8.



718
719
720
721
722
723

Figure 9.